FRACTIONAL LOGARITHMIC SUSCEPTIBLE-INFECTED MODEL. DEFINITION AND APPLICATIONS TO THE STUDY OF COVID-19 MAIN PROTEASE

Luciano Abadias[1,2], Gissell Estrada-Rodriguez[3], Ernesto Estrada[2,4]

Abstract

We propose a model for the transmission of perturbations across the amino acids of a protein represented as an interaction network. The dynamics consists of a Susceptible-Infected (SI) model based on the logarithmic Caputo fractional derivative. We find an approximate analytical solution for this model which represents an upper bound for the fractional SI dynamics on a network. This upper bound is expressed in terms of the Mittag-Leffler function of the adjacency matrix of the network of inter-amino acids interactions. We consider some network descriptors based on these Mittaf-Leffler matrix functions which account for the "circulability" and "transmissibility" of the perturbations across the residues of a protein. We then apply this model and descriptors to the analysis of the communication effects produced by inhibitors of the main protease of COVID-19. We find that the perturbation produced by strong inhibitors of the protease are propagated up to 60Å away from the binding site, confirming the long-range nature of intra-protein communication. These findings may help to the design of drug candidates against this new coronavirus.

MSC 2010: Primary 26A33; Secondary 33E12, 92C40, 05C82

Key Words and Phrases: Caputo derivative; Mittag-Leffler matrix functions; Susceptible-Infected model; COVID-19, SARS CoV-2 protease

1. Introduction

The presence of a networked structure is one of the fundamental characteristics of complex systems in general [10, 19]. It could be argued that

the main function of such networks is that of allowing the communication between the entities that form its structure. In the case of proteins, the non-covalent interactions between residues in their three-dimensional structures form inter-residue networks [10, 17]. These networks facilitate that information about one site is transmitted to and influences the behavior of another. This phenomenon–the transmission of any perturbation in protein structure and function from one site to another–is known as allostery, which represents an essential feature of protein regulation and function [9, 20]. Allostery permits that two residues geometrically distant can interact with each other. As observed experimentally by Ottemann et al. [30] a conformational change of 1Å in a residue can be transmitted to another 100Å apart. As stated long-time ago, such allosteric effects can occur even when the average protein structure remains unaltered [8]. An important kind of allosteric effect is the transmission of the changes produced by a ligand interacting with a protein. Such transmission occurs from the residues proximal to the binding site to other residues distant from it. Such kind of allosteric interaction is very important for understanding the effects of drugs on their receptors, which directly impacts the drug design process [22].

It has been stressed by Berry [7] that there are striking similarities between organization schemes at different observation scales in complex systems, such as allosteric-enzyme networks, cell population and virus spreading. Recently, Miotto et al. [27] exploited these similarities between epidemic spreading and a diffusive process on a protein residue network to prove the capability of propagating information in complex 3D protein[3] structures. Their analogy proved useful in estimating important protein properties ranging from thermal stability to the identification of functional sites [27]. In the current work, we go a step further in the exploitation of the analogy between epidemiological models and communication processes in proteins by considering the inclusion of long-range transmission effects. For this purpose, we develop here a new fractional logarithmic Susceptible-Infected (SI) model for the transmission of perturbations through the amino acids of a protein residue network. Such perturbations are produced, for instance, by the interactions of the given protein with inhibitors, such as drugs or drug candidates. We obtain an upper bound to its exact solution of this fractional logarithmic SI model which is expressed in terms of the Mittag-Leffler matrix functions, and which generalizes the approximate solution found by Lee et al. [21] to the non-fractional (classical) SI model.

Due to its current relevance, we apply the present approach to the study of the long-range inter-residue communication in the main protease of the new coronavirus named SARS-CoV-2 [33, 32]. This new coronavirus

has produced an outbreak of pulmonary disease expanding from the city of Wuhan, Hubei province of China to the rest of the World in about 3 months [35]. One of the most important targets for the development of drugs against SARS-CoV-2 is its main protease, M$^{\text{pro}}$, whose 3-dimensional structure has been recently resolved and deposited [34] in the Protein Data Bank (PDB) [1]. It is a key enzyme for proteolytic processing of polyproteins in the virus and some chemicals have been found to bind this protein, representing potential specific drug canditades against CoV-2 [34]. Here we find that important communication between amino acids in CoV-2 M$^{\text{pro}}$ occurs from the proximities of the binding site to very distant amino acids in other domains of the protein. These effects produced by the interaction with inhibitors are transmistted up to 60Å away from the binding site, confirming the long-range nature of intra-protein communication. According to our results, it seems that stronger inhibitors transmit such perturbations to longer inter-residue distances. Therefore, the current findings are important for the understanding of the mechanisms of drug action on CoV-2 M$^{\text{pro}}$, which may help to the design of drug candidates against this new coronavirus.

2. Antecedents and Motivations

2.1. Protein residue networks

The protein residue networks (PRN) (see ref. [10] Chapter 14 for details) are simple, undirected and connected graphs $G = (V, E)$, where the $v_i \in V, i = 1, \ldots, N$ nodes corresponds to the amino acids of a protein and two nodes v_i and v_j are connected by an edge $\{v_i, v_j\} \in E$ if the corresponding residues (amino acids) interact physically in the protein. They are built here by using the information reported on the Protein Data Bank [1] for the protease of CoV-2 as well as its complexes with three inhibitors (see further). The nodes of the network represent the α-carbon of the amino acids. Then, we consider cutoff radius r_C, which represents an upper limit for the separation between two residues in contact. The distance r_{ij} between two residues i and j is measured by taking the distance between C$_\alpha$ atoms of both residues. Then, when the inter-residue distance is equal or less than r_C both residues are considered to be interacting and they are connected in the PRN. The adjacency matrix A of the PRN is then built with elements defined by

$$A_{ij} = \left\{ \begin{array}{ll} H\left(r_C - r_{ij}\right) & i \neq j, \\ 0 & i = j, \end{array} \right. \tag{2.1}$$

where $H(x)$ is the Heaviside function which takes the value of one if $x > 0$ or zero otherwise. Here we use the typical interaction distance between

two amino acids, which is equal to 7.0Å. We have tested distances below and over this threshold obtaining in general networks which are either too sparse or too dense, respectively.

In this work we consider the structures of the free CoV-2 main protease with PDB code 6Y2E as well as the ones of the CoV-2 with inhibitors O6K (6Y2F and 6Y2G) [34], N3 (6LU7) [18] and X77 (6W63) [26]. The structures in 6Y2F and 6Y2G, which correspond to the same inhibitor, differ in their space groups: $C2$ for 6Y2F and $P2_12_12_1$ for 6Y2G [34]. The EC_{50} of an inhibitor refers to the concentration of the inhibitor which induces a response halfway between the baseline and maximum after a specified exposure time. The smallest the value of EC_{50}, the more potent the inhibitor is.

2.2. Standard SI model

Here we state the main motivation of using a Susceptible-Infected (SI) model for studying the effects of inhibitor binding to a protein residue network in a similar way as an SIS has been used by Miotto et al. [27]. The selection of an SI model can be understood by the fact that we are interested in the early times of the dynamics. At this stage, it has been shown [21] that the SI model is most suitable than any other model. To motivate the SI model in the PRN context let us consider that an amino acid is in the binding site of a protein. Then, this amino acid is susceptible to be perturbed by the interaction with this inhibitor. Consequently, this residue can be in one of two states, either waiting to be perturbed (susceptible) or being perturbed by the interaction. Of course, this amino acid can transmit this perturbation to any other amino acid in the protein to which it interacts with. Then, if β is the rate at which such perturbation is transmitted between amino acids, and if $s_i(t)$ and $x_i(t)$ are the probabilities that the residue i is susceptible or get perturbed at time t, respectively, we can write the dynamics

$$\frac{ds_i(t)}{dt} = -\beta s_i(t) x_i(t), \tag{2.2}$$

$$\frac{dx_i(t)}{dt} = \beta s_i(t) x_i(t). \tag{2.3}$$

Because the amino acids can only be in the states "susceptible" or "perturbed" we have that $s_i(t) + x_i(t) = 1$, such that we can write

$$\frac{dx_i(t)}{dt} = \beta(1 - x_i(t)) x_i(t). \tag{2.4}$$

When we consider all the interactions between pairs of residues in the PRN we should transform the previous equation into a system of equations of the following form [25]:

$$\frac{dx_i(t)}{dt} = \beta\left(1 - x_i(t)\right) \sum_{j \in \mathcal{N}} A_{ij} x_j(t), t \geqslant t_0, \qquad (2.5)$$

where A_{ij} are the entries of the adjacency matrix of the PRN for the pair of amino acids i and j, and $\mathcal{N}$ is the set of nearest neighbors of j. In matrix-vector form becomes:

$$\frac{dx(t)}{dt} = \beta\left[I_N - \mathrm{diag}\left(x(t)\right)\right] A x(t), \qquad (2.6)$$

with initial condition $x(0) = x_0$. The evolution of dynamical systems based on the adjacency matrix of a network have been analyzed by Mugnolo [29]. It is well-known that [21]:

(1) if $x_0 \in [0,1]^n$ then $x(t) \in [0,1]^n$ for all $t > 0$;
(2) $x(t)$ is monotonically non-decreasing in t;
(3) there are two equilibrium points: $x^\star = 0$, i.e. no epidemic, and $x^\star = 1$, i.e. full contagion;
(4) the linearization of the model around the point 0 is given by

$$\frac{dx(t)}{dt} = \beta A x(t), \qquad (2.7)$$

    and it is exponentially unstable;
(5) each trajectory with $x_0 \neq 0$ converges asymptotically to $x^\star = 1$, i.e. the epidemic spreads monotonically to the entire network.

The SI model can be rewritten as

$$\frac{1}{1 - x_i(t)} \frac{dx_i(t)}{dt} = \beta \sum_{j \in \mathcal{N}} A_{ij} \left(1 - e^{-(-\log(1 - x_j(t)))}\right), \qquad (2.8)$$

which is equivalent to

$$\frac{dy_i(t)}{dt} = \beta \sum_{j \in \mathcal{N}} A_{ij} f\left(y_j(t)\right), \qquad (2.9)$$

where $y_i(t) := g\left(x_i(t)\right) = -\log\left(1 - x_i(t)\right) \in [0, \infty]$, $f(y) := 1 - e^{-y} = g^{-1}(y)$.

Lee et al. [21] have considered the following linearized version of the previous nonlinear equation

$$\frac{d\hat{y}(t)}{dt} = \beta A \mathrm{diag}\left(1 - x(t_0)\right) \hat{y}(t) + \beta b\left(x(t_0)\right), \qquad (2.10)$$

where $\hat{x}(t) = f(\hat{y}(t))$ in which $\hat{x}(t)$ is the approximate solution to the SI model, $\hat{y}(t_0) = g(x(t_0))$ and $b(x) := x + (1-x)\log(1-x)$. They have found that the solution to this linearized model is [21]:

$$\hat{y}(t) = e^{\beta(t-t_0)A\mathrm{diag}(1-x(t_0))}g(x(t_0))$$
$$+ \sum_{k=0}^{\infty} \frac{(\beta(t-t_0))^{k+1}}{(k+1)!} [A\mathrm{diag}(1-x(t_0))]^k Ab(x(t_0)). \qquad (2.11)$$

When $t_0 = 0$, $x_i(0) = c/N$, $i = 1, 2, \ldots, N$ for some c, the previous equation is transformed to

$$\hat{y}(t) = (1/\eta - 1)e^{\eta\beta tA}\vec{1} - (1/\eta - 1 + \log(\eta))\vec{1}, \qquad (2.12)$$

where $\eta = 1 - c/N$ and $\vec{1}$ is the all-ones vector. Lee et al. [21] have proved that this solution is an upper bound to the exact solution of the SI model. This result indicates that the upper bound to the solution of the SI model is proportional to the exponential of the adjacency matrix of the network, which is the source of the subgraph centrality [13] and of the communicability function [12] between pairs of nodes in it. In the next section of this work we obtain a generalization of this upper bound based on a fractional logarithmic SI model, which will also be formulated there.

3. Mathematical Results

3.1. Definition of the logarithmic fractional SI model

In the following we will consider a fractional SI model based on the fractional derivative of the logarithmic function of x_i (probability that the residue i get perturbed at time t), that we will call fractional logarithmic derivative.

First of all, we recall the definition of Caputo fractional derivative. Given $0 < \alpha < 1$ and a function $u : [0, \infty) \to \mathbb{R}$, we denote by $D_t^{\alpha}u$ the fractional Caputo derivative of u of order α, which is given by [23]

$$D_t^{\alpha}u(t) = \int_0^t g_{1-\alpha}(t-\tau)u'(\tau)\,d\tau := (g_{1-\alpha} * u')(t), \quad t > 0,$$

where $*$ denotes the classical convolution product on $(0, \infty)$ and $g_{\gamma}(t) := \frac{t^{\gamma-1}}{\Gamma(\gamma)}$, for $\gamma > 0$. Observe that the previous fractional derivative has sense whenever the function is derivable and the convolution is defined (for example if u' is locally integrable). The notation g_{γ} is very useful in the fractional calculus theory, mainly by the property $g_{\gamma} * g_{\delta} = g_{\gamma+\delta}$ for all $\gamma, \delta > 0$.

Before to present our model, we state a technical lemma which plays a key role in the main result of this section.

LEMMA **3.1**. *Let $u : [0, \infty) \to \mathbb{R}$ be a derivable function with $u(0) = 0$, and $0 < \alpha < 1$. If $D_t^\alpha u(t) \geqslant 0$ for all $t > 0$, then $u(t) \geqslant 0$.*

P r o o f. Observe that by hypothesis $(g_{1-\alpha} * u')(t) \geqslant 0$, therefore

$$u(t) = \int_0^t u'(\tau)\, d\tau = (g_1 * u')(t) = (g_\alpha * g_{1-\alpha} * u')(t) \geqslant 0.$$

$\square$

Now, we recall that β will denote the perturbation rate and let $s_i(t)$ and $x_i(t)$ be the probabilities that residue i is susceptible or get perturbed at time t, respectively. Let $0 < \alpha < 1$, we consider the following fractional model inspired by (2.2) and (2.3):

$$\begin{cases} \displaystyle \int_0^t g_{1-\alpha}(t-\tau)\, \frac{s_i'(\tau)}{x_i(\tau)}\, d\tau = -\beta^\alpha s_i(t), \\[2ex] \displaystyle \int_0^t g_{1-\alpha}(t-\tau)\, \frac{x_i'(\tau)}{s_i(\tau)}\, d\tau = \beta^\alpha x_i(t). \end{cases}$$

If we assume $s_i(t) + x_i(t) = 1$, we have

$$\int_0^t g_{1-\alpha}(t-\tau)\, \frac{x_i'(\tau)}{1 - x_i(\tau)}\, d\tau = \beta^\alpha x_i(t). \tag{3.13}$$

Observe that the left-hand side of the above system is the fractional logarithmic derivative (see for instance [28]), that is,

$$D_t^\alpha(-\log(1 - x_i))(t).$$

As in the classical SI model happens, this equation is transformed into a system of equations when we consider the interactions between the different residues in the protein according to the PRN. So, the fractional SI model which we will study is given by

$$\int_0^t g_{1-\alpha}(t-\tau)\, \frac{x_i'(\tau)}{1 - x_i(\tau)}\, d\tau = \beta^\alpha \sum_{j \in \mathcal{N}} A_{ij} x_j, \quad i \in \mathcal{N}, t > 0, x_i(0) \in [0, 1].$$

$$\tag{3.14}$$

We can rewrite (3.14) in a matrix-vector form:

$$D_t^\alpha(-\log(1 - x))(t) = \beta^\alpha A x(t), \tag{3.15}$$

with initial condition $x(0) = x_0$. This fractional SI model, based on the fractional logarithmic derivative, has not been considered in the literature

under our knowledge. Other fractional compartmental models have been previously discussed in the literature (see for instance [4] and references therein).

Note that if $x_i(0) = 1$, then by (3.14) we have $\dfrac{x_i'(\tau)}{1 - x_i(\tau)} \geqslant 0$ for s close to 0, and that case is not possible. So, we will consider that $x_i^\star = 1$ is an equilibrium point. The same happens if $x_i^\star = 0$ by the equations given by s_i. Furthermore, if $x_i(0) \in (0, 1)$, by Lemma **3.1** we have $-\log(1 - x_i(t)) \geqslant -\log(1 - x_i(0)) > 0$, then $x_i(t) \in (0, 1)$, and therefore x_i is non-decreasing. We deduce that if $x(0) \in [0, 1]^n$ then $x(t) \in [0, 1]^n$ for all $t > 0$, and there are two equilibrium points: $x^\star = 0$, i.e. no epidemic, and $x^\star = 1$, i.e., full contagion. Also, each trajectory with $x_0 \neq 0$ converges asymptotically to $x^\star = 1$, i.e. the epidemic spreads monotonically to the entire network.

The linearized problem

$$D_t^\alpha \tilde{x}(t) = \beta^\alpha A\tilde{x}(t)$$

is unstable. In fact, the solution is

$$\tilde{x}(t) = E_{\alpha,1}\left(((\beta t)^\alpha A\right) x_0 := \sum_{n=0}^\infty \frac{(\beta t)^{\alpha n} A^n x_0}{\Gamma(\alpha n + 1)}, \qquad (3.16)$$

where x_0 is the same initial condition that in the non-linearized problem.

Note that the fractional SI model can be rewritten as

$$D_t^\alpha y_i(t) = \beta^\alpha \sum_{j \in \mathcal{N}} A_{ij} f(y_j(t)),$$

where $y_i(t) := g(x_i(t)) = -\log(1 - x_i(t)) \in [0, \infty)$, and $f(y) = 1 - e^{-y} = g^{-1}(y)$.

Now we consider the Lee-Tenneti-Eun (LTE) transformation [21] which produces the following linearized equation

$$D_t^\alpha \hat{y}(t) = \beta^\alpha A\mathrm{diag}(1 - x_0)\hat{y}(t) + \beta^\alpha Ab(x(0)), \qquad (3.17)$$

where $\hat{x}(t) = f(\hat{y}(t))$ in which $\hat{x}(t)$ is an approximate solution to the fractional SI model, $\hat{y}$ is the solution of (3.17) with initial condition $\hat{y}(0) = g(x(0))$ and $b(x) := x + (1 - x)\log(1 - x)$. For convenience, we write $\Omega := \mathrm{diag}(1 - x_0)$, and $\hat{A} = A\Omega$.

THEOREM **3.2**. *For any $t \geqslant 0$, we have*

$$x(t) \leq \hat{x}(t) = f(\hat{y}(t)) \leq \tilde{x}(t),$$

under the same initial conditions $x_0 := x(0) = \hat{x}(0) = \tilde{x}(0)$, where the solution $\hat{y}$ of (3.17) is given by

$$\hat{y}(t) = E_{\alpha,1}\left((\beta t)^\alpha \hat{A}\right) g(x_0) + \sum_{n=0}^{\infty} \frac{(\beta t)^{\alpha(n+1)} \hat{A}^n A b(x_0)}{\Gamma(\alpha(n+1)+1)}, \qquad (3.18)$$

and $\tilde{x}$ is given by (3.16). Furthermore, $\|\hat{x}(t) - x(t)\| \to 0$ and $\|\tilde{x}(t) - x(t)\| \to \infty$ as t goes to infinity.

P r o o f. First of all, by the theory of fractional calculus, it is well-known that the solution of the linearized problem (3.17) is given

$$\hat{y}(t) = E_{\alpha,1}\left((\beta t)^\alpha \hat{A}\right) g(x_0) + \int_0^t \tau^{\alpha-1} E_{\alpha,\alpha}\left((\beta s)^\alpha \hat{A}\right) \beta^\alpha A b(x(0)) \, d\tau.$$

$$(3.19)$$

On the above,

$$E_{\alpha,1}\left((\beta t)^\alpha \hat{A}\right) x_0 := \sum_{n=0}^{\infty} \frac{(\beta t)^{\alpha n} \hat{A}^n x_0}{\Gamma(\alpha n + 1)}, \quad t^{\alpha-1} E_{\alpha,\alpha}\left((\beta t)^\alpha \hat{A}\right) := t^{\alpha-1} \sum_{n=0}^{\infty} \frac{(\beta t)^{\alpha n} \hat{A}^n}{\Gamma(\alpha n + \alpha)}.$$

Therefore, since

$$\int_0^t \tau^{\alpha n + \alpha - 1} \, d\tau = \frac{t^{\alpha n + \alpha}}{\alpha n + \alpha},$$

from (3.19) we get (3.18). For more details about linear fractional models see [2, 3, 5], and references therein. Notice that Eq. (3.18) is the generalized fractional version of the one obtained by LTE by means of their Theorem **3.2**. Their specific solution is recovered when $\alpha = 1$ where $E_{1,1}\left(\beta t \hat{A}\right) = \exp\left(\beta t \hat{A}\right)$ and $\Gamma(n+2) = (n+1)!$.

We have assumed that $x_0 = x(0) = \hat{x}(0) = \tilde{x}(0)$, with $y(t) = g(x(t))$ and $\hat{y}(t) = g(\hat{x}(t))$. Since $y, \hat{y}$ are non-decreasing functions of $x, \hat{x}$, it is enough to prove that $y(t) \le \hat{y}(t)$ to get $x(t) \le \hat{x}(t)$. Following the paper of Lee et all, since f is a concave function with $f'(y) = e^{-y}$, we have

$$D_t^\alpha y_i(t) \leqslant \beta^\alpha \sum_{j \in \mathcal{N}} A_{ij}(1 - x_j(0)) y_j(t) + \beta^\alpha \sum_{j \in \mathcal{N}} A_{ij} b(x_j(0)).$$

Then, since $y(0) = \hat{y}(0)$, $D_t^\alpha y(t) \le D_t^\alpha \hat{y}(t)$, so Lemma **3.1** implies $x(t) \le \hat{x}(t)$.

Now, note that

$$D_t^\alpha \hat{x}_i(t) = D_t^\alpha f(\hat{y}_i(t)) = \int_0^t g_{1-\alpha}(t - s) e^{-\hat{y}_i(s)} \hat{y}_i'(s) \, ds.$$

Furthermore (3.18) shows that $y_i'(s) \geqslant 0$ for all $s > 0$, then

$$0 \leqslant D_t^\alpha \hat{x}_i(t) \leqslant \int_0^t g_{1-\alpha}(t-s)\,\hat{y}_i'(s)\,ds = D_t^\alpha \hat{y}_i(t).$$

Also, it is well-known (see for example [2, 3, 5]) that the previous Mittag-Leffler matrix functions satisfy

$$E_{\alpha,1}\left((\beta t)^\alpha \hat{A}\right) = \left(g_{1-\alpha} * s^{\alpha-1} E_{\alpha,\alpha}\left((\beta s)^\alpha \hat{A}\right)\right)(t)$$

$$= \int_0^t g_{1-\alpha}(t-s)\,s^{\alpha-1} E_{\alpha,\alpha}\left((\beta s)^\alpha \hat{A}\right)\,ds \qquad (3.20)$$

and

$$E_{\alpha,1}\left((\beta t)^\alpha \hat{A}\right) I = I + \beta^\alpha \hat{A}\left(g_\alpha * E_{\alpha,1}\left((\beta s)^\alpha \hat{A}\right)\right)(t)$$

$$= I + \beta^\alpha \hat{A} \int_0^t g_\alpha(t-s)\, E_{\alpha,1}\left((\beta s)^\alpha \hat{A}\right)\,ds. \qquad (3.21)$$

Then, by (3.17), (3.19), (3.20) and (3.21) one gets

$$
\begin{aligned}
D_t^\alpha \hat{y}(t) &= \beta^\alpha \hat{A} E_{\alpha,1}\left((\beta t)^\alpha \hat{A}\right) g(x_0) + \beta^\alpha \hat{A}\left(g_1 * s^{\alpha-1} E_{\alpha,\alpha}\left((\beta s)^\alpha \hat{A}\right)\right)(t) \\
&\times \quad \beta^\alpha Ab(x(0)) + \beta^\alpha Ab(x(0)) \\
&= \beta^\alpha \hat{A} E_{\alpha,1}\left((\beta t)^\alpha \hat{A}\right) g(x_0) + \beta^\alpha \hat{A}\left(g_\alpha * g_{1-\alpha} * s^{\alpha-1} E_{\alpha,\alpha}\left((\beta s)^\alpha \hat{A}\right)\right)(t) \\
&\times \quad \beta^\alpha Ab(x(0)) + \beta^\alpha Ab(x(0)) \\
&= \beta^\alpha \hat{A} E_{\alpha,1}\left((\beta t)^\alpha \hat{A}\right) g(x_0) + \beta^\alpha \hat{A}\left(g_\alpha * E_{\alpha,1}\left((\beta s)^\alpha \hat{A}\right)\right) \\
&\times \quad (t)\,\beta^\alpha Ab(x(0)) + \beta^\alpha Ab(x(0)) \\
&= \beta^\alpha \hat{A} E_{\alpha,1}\left((\beta t)^\alpha \hat{A}\right) g(x_0) + E_{\alpha,1}\left((\beta t)^\alpha \hat{A}\right) \beta^\alpha Ab(x(0)) \\
&= \beta^\alpha A E_{\alpha,1}\left((\beta t)^\alpha \hat{A}\right) x(0),
\end{aligned}
$$

where in the last equality we have used that $\Omega g(x(0)) + b(x(0)) = x(0)$. By definition of Mittag-Leffler matrix function, it is easy to see that

$$E_{\alpha,1}\left((\beta t)^\alpha \hat{A}\right) x(0) \leq E_{\alpha,1}\left((\beta t)^\alpha A\right) x(0),$$

since $\hat{A} = A\Omega$ with $\Omega = \mathrm{diag}\,(1 - x(0))$. Therefore

$$D_t^\alpha \hat{x}(t) \leq D_t^\alpha \hat{y}(t) \leq \beta^\alpha A E_{\alpha,1}\left((\beta t)^\alpha A\right) x(0) = D_t^\alpha \tilde{x}(t),$$

and Lemma **3.1** implies $\hat{x}(t) \leq \tilde{x}(t)$.

Finally, it is known that $\lim_{t\to\infty} \tilde{x}_i(t) = \infty$ and $\lim_{t\to\infty} \hat{y}_i(t) = \infty$. Since f is continuous, $\lim_{t\to\infty} \hat{y}_i(t) = \infty$, then $\lim_{t\to\infty} \hat{x}_i(t) = \lim_{t\to\infty} f(\hat{y}_i)(t) = 1$. Therefore, since $\lim_{t\to\infty} x_i(t) = 1$ we conclude $\|\hat{x}(t) - x(t)\| \to 0$ and $\|\tilde{x}(t) - x(t)\| \to 0$ as $t \to \infty$. $\qquad \square$

COROLLARY **3.3**.   *Let $x_0 \leq 1$, then the solution of (3.17) can be written as*

$$\hat{y}(t) = g(x_0) + \left[E_{\alpha,1}\left((\beta t)^\alpha \hat{A}\right) - I \right] \Omega^{-1} x(0). \qquad (3.22)$$

P r o o f. Let us write Eq. (3.19) in the following way

$$\hat{y}(t) = E_{\alpha,1}\left((\beta t)^\alpha \hat{A}\right) g(x_0) + \int_0^t s^{\alpha-1} E_{\alpha,\alpha}\left((\beta s)^\alpha \hat{A}\right) \beta^\alpha A\Omega\Omega^{-1} b(x(0))\, ds, \qquad (3.23)$$

which can be reordered as

$$\hat{y}(t) = E_{\alpha,1}\left((\beta t)^\alpha \hat{A}\right) g(x_0) + \left[\beta^\alpha \hat{A} \int_0^t s^{\alpha-1} E_{\alpha,\alpha}\left((\beta s)^\alpha \hat{A}\right) ds \right] \Omega^{-1} b(x(0)). \qquad (3.24)$$

So, by (3.21) we have

$$\hat{y}(t) = E_{\alpha,1}\left((\beta t)^\alpha \hat{A}\right) g(x_0) + \left[E_{\alpha,1}((\beta t)^\alpha \hat{A}) - I \right] \Omega^{-1} b(x(0)). \qquad (3.25)$$

Now, it is easy to check that $\Omega^{-1} b(x(0)) = \Omega^{-1} x(0) - g(x_0)$. Therefore,

$$\hat{y}(t) = E_{\alpha,1}\left((\beta t)^\alpha \hat{A}\right) \Omega^{-1} x(0) - \Omega^{-1} x(0) + g(x_0), \qquad (3.26)$$

which by reordering gives the final solution. $\square$

Let us now consider $x_0 = \frac{c}{N}$ where $c \in \mathbb{R}^+$, let $\gamma = 1 - x_0$. Noting that $\mathrm{diag}(1 - x(0)) = \gamma I$, then

$$\begin{aligned}
\hat{y}(t) &= \left(\frac{1-\gamma}{\gamma}\right) E_{\alpha,1}\left(t^\alpha \beta^\alpha \hat{A}\right) \vec{1} - \left(\frac{1-\gamma}{\gamma} + \log\gamma\right) \vec{1} \\
&= \left(\frac{1-\gamma}{\gamma}\right) E_{\alpha,1}\left(t^\alpha \beta^\alpha A\mathrm{diag}(1-x(0))\right)\vec{1} - \left(\frac{1-\gamma}{\gamma} + \log\gamma\right)\vec{1} \\
&= \left(\frac{1-\gamma}{\gamma}\right) E_{\alpha,1}\left(t^\alpha \beta^\alpha \gamma A\right)\vec{1} - \left(\frac{1-\gamma}{\gamma} + \log\gamma\right)\vec{1}. \qquad (3.27)
\end{aligned}$$

3.2. On Mittag-Leffler matrix functions

The Mittag-Leffler function $E_{\alpha,1}\left(\zeta A\right)$ with $\zeta = (\beta t)^{1/2}\gamma$, which appears in the approximate solution of the fractional logarithmic SI model, belongs to the class of matrix functions of the adjacency matrix [6]. They have been widely used to analyze the structure of complex networks [6]. In general, it can be written as [24, 16, 31, 15]

$$E_{\alpha,\nu}\left(\zeta A\right) = \sum_{k=0}^{\infty} \frac{(\zeta A)^k}{\Gamma\left(\alpha k + \nu\right)}, \alpha > 0, \nu \in \mathbb{C}. \qquad (3.28)$$

The properties of these matrix functions and its computational implementation have been previously studied. Based on previous empirical findings [11] for the analysis of the main protease of CoV-2 we will consider here the specific case where $\alpha = 1/2$ and $\nu = 1$. In this particular case, the Mittag-Leffler function which appears in the solution of our fractional logarithmic SI model can be written as

$$E_{1/2,1}\left(\zeta A\right) = \sum_{k=0}^{\infty} \frac{(\zeta A)^k}{\Gamma\left(\frac{k}{2}+1\right)} = \sqrt{\frac{\pi}{2}} \sum_{k=0}^{\infty} \frac{\left(\frac{1}{\sqrt{2}}\zeta A\right)^k}{k!!}, \qquad (3.29)$$

where $k!!$ is the double factorial, which is equivalent to the matrix function previously studied by Silver and Estrada [14]. This is important to understand structurally the meaning of our solution in relation to the one of the classical SI which is based on the matrix exponential [13, 12]. In the matrix exponential $\exp\left(\zeta A\right)$ the powers of the adjacency matrix are divided by the simple factorial, $\exp\left(\zeta A\right) = \sum_{k=0}^{\infty} (\zeta A)^k / k!$. To understand the structural meaning of these expressions we need the following (see [10]).

THEOREM **3.4**. *The number of walks of length k between the nodes i and j of the graph G is given by $\left(A^k\right)_{ij}$.*

A *walk* of length k in G is a set of nodes $i_1, i_2, \ldots, i_k, i_{k+1}$ such that for all $1 \leqslant l \leqslant k$, $(i_l, i_{l+1}) \in E$. A *closed walk* is a walk for which $i_1 = i_{k+1}$ [10]. Therefore, the functions $E_{1/2,1}\left(\zeta A\right)$ and $\exp\left(\zeta A\right)$ counts the walks of any lengths from different pairs of residues in the protein, but the first penalizes such walks by the double factorial of its length and the second penalizes them by the single factorial. The double factorial growths more slowly than the single one, which means that the longer walks in $E_{1/2,1}\left(\zeta A\right)$ are less penalized than in $\exp\left(\zeta A\right)$. In other words, the function $E_{1/2,1}\left(\zeta A\right)$ accounts for more long-range interactions between amino acids in a protein than the matrix exponential, which means that the fractional logarithmic SI model describes a longer-range process than the classical SI one.

For the analysis of specific problems we can split the network structural contributions to the fractional SI model as

$$\mathscr{R}_i = (E_{\alpha,1}\left(\zeta A\right))_{ii} + \sum_{j} (E_{\alpha,1}\left(\zeta A\right))_{ij} = \hat{\mathscr{C}}_i + \hat{\mathscr{T}}_i, \qquad (3.30)$$

where $\hat{\mathscr{C}}_i$ represents the "circulability" of the infectious particle around the node i of the network and $\hat{\mathscr{T}}_i$ represents the capacity of this node to transmit the infectious particle to any other node of the network, i.e., its "transmissibility". In particular, the individual terms $G_{ij}^{\alpha} = (E_{\alpha,1}(\zeta A))_{ij}$ represents the fractional communicability of the nodes i and j in the network. In this work, we will make emphasis on the fractional communicability between amino acids in the main protease of CoV-2 as a way of quantifying the inter-residue communication and the influence of inhibitors on it.

4. Computational Results

We start this section by comparing the time evolution of the SI dynamics under the normal and fractional approaches using the upper bound obtained here. That is, because the approximate solution to the fractional SI model obtained here, namely

$$\hat{y}(t) = \left(\frac{1-\gamma}{\gamma}\right) E_{\alpha,1}\left(t^{\alpha}\beta^{\alpha}\gamma A\right)\vec{1} - \left(\frac{1-\gamma}{\gamma} + \log\gamma\right)\vec{1}, \qquad (4.31)$$

generalizes the result obtained by Lee et al. we use it to compare the results using different values of the Mittag-Leffler function. In particular we study here $\alpha = 1$ (normal SI) and $\alpha = \frac{1}{2}$. In Fig. **4.1** we illustrate the time evolution of the SI dynamics using these parameters for CoV-2 M$^{\text{pro}}$ with three different inhibitors as explained before. In both cases we used the same set of parameters, namely $\beta = 0.01$, $\gamma = 1 - \frac{c}{N}$, $c = 0.005$. Therefore, the differences in the dynamics are only due to the fractional nature of the evolution equations used in each case. As can be seen the time needed to perturb all the amino acids of the protease is about ten times smaller when $\alpha = \frac{1}{2}$ than when $\alpha = 1$. This means that in a normal diffusive process like the one when $\alpha = 1$ a perturbation occurring at a given region of the protease is slowly transmitted to the rest of the residues in the protein. In contrast, when the diffusive process is of fractional nature, such transmission is almost instantaneous across the whole structure of the protein. Unfortunately, we do not have experimental facts that support one or the other mechanism at this time.

In order to gain more insights about the influence of the two different dynamics on the propagation of a perturbation across the CoV-2 M$^{\text{pro}}$ when bounded with inhibitors we study the structural contributions from each of the structures to the SI dynamics. That is, we study the terms of the matrix Mittag-Leffler function which appears in the solution of the generalized SI model, which is the one containing all the structural information about the protein by means of the adjacency matrix A. We namely calculate the
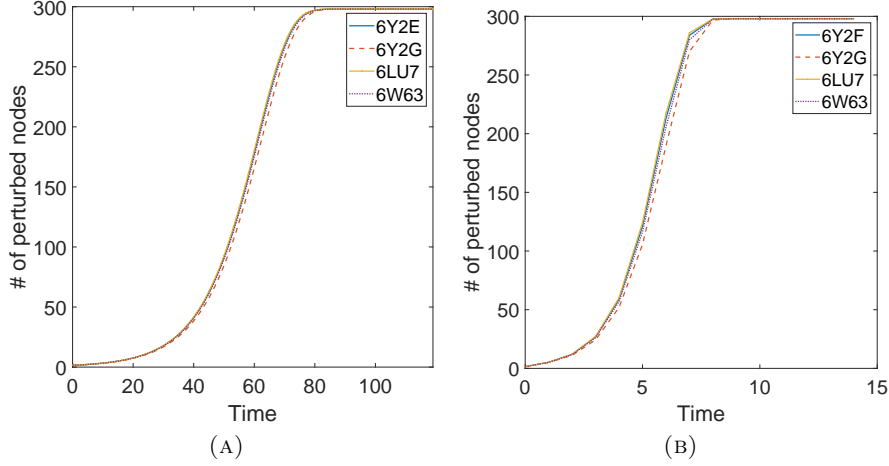
FIGURE **4.1.** Time evolution of the upper bounds of the normal (A) and fractional (B) SI model for the main protease of CoV-2 bounded to inhibitors with $\beta = 0.01$, $\gamma = 1 - \frac{c}{N}$, $c = 0.005$.

relative differences in the circulability of the perturbation around a given amino acid G_{ii}^{α}, as well as the individual components of the transmissibility of this perturbation from one residue to another, G_{ij}^{α}. These relative changes are defined by

$$\Delta G_{ii}^{\alpha} = \frac{1}{N} \sum_{i=1}^{N} \frac{G_{ii}^{\alpha} \,(\text{bounded}) - G_{ii}^{\alpha} \,(\text{free})}{G_{ii}^{\alpha} \,(\text{free})}, \qquad (4.32)$$

$$\Delta G_{ij}^{\alpha} = \frac{1}{N \,(N-1)} \sum_{i \neq j} \frac{G_{ij}^{\alpha} \,(\text{bounded}) - G_{ij}^{\alpha} \,(\text{free})}{G_{ij}^{\alpha} \,(\text{free})}. \qquad (4.33)$$

Because the dynamics with different fractional exponents runs at very different rates, we have to select different times for the calculations of these relative changes. We have selected the time at which 50% of the amino acids in the protease are perturbed, which occurs at $t = 6$ for $\alpha = 1/2$ and $t = 50$ for $\alpha = 1$. The rest of the parameters remain the same for both descriptors, i.e., $\beta = 0.01$, $\gamma = 1 - \frac{c}{N}$, $c = 0.005$. In Table 1 we give the values of the relative changes in both parameters expressed as percentage. The first interesting result is that when $\alpha = 1$ the most significant changes in the protease structures bounded to inhibitors occurs in the neighborhood of the amino acids. That is the circulability of the perturbation around the residues, $\Delta G_{ii}^{\alpha=1}$, is more than 300% larger in the bounded protease than

Inhibitor	$\Delta G_{ii}^{\alpha=1}$ (%)	$\Delta G_{ij}^{\alpha=1}$ (%)	$\Delta G_{ii}^{\alpha=1/2}$ (%)	$\Delta G_{ij}^{\alpha=1/2}$ (%)	EC$_{50}$ (μM)
6Y2F	326.6	353.5	77.4	675.5	0.67
6Y2G	307.3	57.2	49.9	243.4	
6LU7	329.0	87.2	69.9	393.1	16.77
6W63	324.1	110.0	64.1	385.0	

TABLE 1. Change of circulability and of the individual transmissibility of perturbations between amino acids in CoV-2 M$^{\text{pro}}$ bounded to inhibitors relative to the free protease.

in the free one. This contrast with what we observe for the transmissibility terms, $\Delta G_{ij}^{\alpha=1}$, which, with the exception of 6Y2F, have less than $1/3$ of variation than that of the circulability. These results contrast dramatically with those obtained for $\alpha = 1/2$. In this case, the circulability is only about 60% larger in the bounded protease than in the free one. However, here the individual transmissibilities are about 300% higher in the bounded protease than in the free one. Here again 6Y2F is an exception with almost 700% of increment. We remind the reader that the structures 6Y2F and 6Y2G contain the same inhibitor and their difference is due to the different space group in which the structures are resolved [34]. The structure 6Y2F is in the same space group as the free protease, namely $C2$, where both protomers A and B have identical conformations. However, 6Y2G is in the space group $P2_12_12_1$, where the two protomers have different conformations. It was noticed by Zhang et al. [34] that in 6Y2G "*the key residue Glu166 adopts an inactive conformation in protomer B*" even though the inhibitor "*is bound in the same mode*" in both protomers. Therefore, we consider the hypothesis that the "correct" structure for the inhibitor studied by Zhang et al. is the one with the code 6Y2F and not the one with PDB code 6Y2G. The inhibitor studied by Zhang et al. [34] is a very potent one, with EC$_{50}$ of 0.67 μM. Notice that the inhibitor in 6LU7 has EC$_{50}$ 25 times higher than that of 6Y2F. We should expect then that the effects of this potent inhibitor in 6Y2F are "felt" by very distant amino acids in CoV-2 M$^{\text{pro}}$. This is exactly what is reflected by the values of $\Delta G_{ij}^{\alpha=1/2}$. While the increase of this transmissibility in 6LU7 and 6W63 is more than 350% relative to the free protease, such increment is almost 700% in 6Y2F. In contrast, the relative increase of the transmissibility in 6Y2G is smaller than that in 6LU7 and 6W63.

We proceed now with the analysis of the individual pairs of amino acids with the largest values of $\Delta G_{ij}^{\alpha=1/2}$. These are the pairs of residues for which the transmissibility of a perturbation increased the most after the

rank	i	j	$\Delta G_{ij}^{\alpha=1/2}$	l_{ij}	d_{ij} (Å)
1	H64	S284	430.3	9	46.6
2	H64	N221	359.8	13	62.9
3	E55	S284	280.7	10	47.0
4	T93	S284	275.8	9	43.6
5	K61	S284	263.2	10	50.9
6	K97	N221	260.2	10	48.7
7	P96	**Q192**	256.9	8	34.6
8	H64	Q110	256.5	6	29.6
9	T93	N221	254.3	12	56.7
10	H64	E288	254.1	7	37.6
mean				9.2 ± 2.0	45.8 ± 9.5

TABLE 2. Pairs of amino acids i, j with the largest variation of $\Delta G_{ij}^{\alpha=1/2}$ in 6Y2F. The length of the shortest paths l_{ij} between the two nodes as well as the distance between the C_α of both amino acids, d_{ij} (Å), are also given. Amino acids in the binding site or directly bounded to a residue in it are marked in bold.

interaction of CoV-2 M^{pro} with the corresponding inhibitor. In Table 2 we show the top ten pairs of amino acids by their values of $\Delta G_{ij}^{\alpha=1/2}$. In all these cases the relative change of the individual transmissibility is positive, which means that the transmissibility of these pairs of residues is much higher in the bounded protease than in the free one. As can be seen in Table 2, the transmissibility increase in 6Y2F relative to 6Y2E is between 250 to 430 times bigger that the individual transmissibility in the free protease. This is a huge increase in the transmissibility of perturbations across the structure of CoV-2 M^{pro} after being bounded to the inhibitor O6K. To corroborate the long-distance nature of these transmissions, we calculated the shortest path length between these residues and the corresponding geometric inter-residue distance in the protease. As can be seen in Table 2, these pairs of residues are separated by an average of 9.2 ± 2.0 steps, i.e., the number of intermediate residues between the two endpoints is between 5 and 11. More importantly, the geometric separation between these pairs of residues range between 30 and 62Å, with an average of 45.8 ± 9.5Å, which is a significantly large inter-residue separation. Notice that the longer separation between a pair of residues in the CoV-2 M^{pro} is about 69Å, which implies that the average transmissibility detected by $\Delta G_{ij}^{\alpha=1/2}$ is about 2/3 of the maximum possible one.
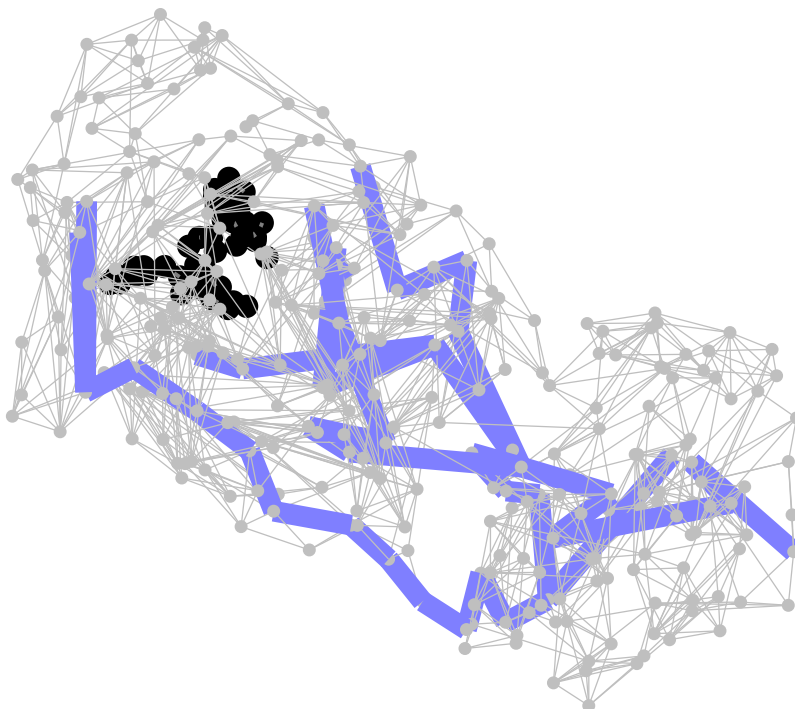
FIGURE **4.2.** Visualization of the PRN of CoV-2 main protease with inhibitor having PDB code 6Y2F. The paths marked in blue correspond to the shortest paths between pairs of nodes that increase their fractional communicability respect to the free protease (see Table 2). The inhibitor is marked in black.

In Fig. **4.2** we illustrate the shortest paths connecting the pairs of amino acids with the top ten largest values of $\Delta G_{ij}^{\alpha=1/2}$ in the CoV-2 M$^{\mathrm{pro}}$ bounded with the inhibitor O6K.

The case of 6Y2G is very different from that of 6Y2F not only because the amino acids in the top ten ranking are different, but mainly because the average separation between these residues is significantly smaller than the ones in 6Y2F. In Table 3 we gives the values of the geometric distance between the pairs of amino acids with the largest values of $\Delta G_{ij}^{\alpha=1/2}$ in the CoV-2 protease bounded to O6K. As can be seen the average separation between these residues is 22% smaller than that in 6Y2F, which means that the average transmissibility between amino acids in this structure is 10Å less than in 6Y2F. This average separation of the amino acids is similar to the one observed for the case of 6LU7 (see further), which corresponds

rank	i	j	$\Delta G_{ij}^{\alpha=1/2}$	l_{ij}	d_{ij} (Å)
1	**L167**	M276	150.6	8	31.7
2	L177	M276	121.2	9	40.6
3	R76	M276	119.2	12	57.9
4	S139	M276	97.5	7	28.2
5	G183	M276	93.5	8	33.3
6	G138	M276	89.9	6	26.5
7	A173	M276	69.0	7	32.3
8	**L167**	N221	65.2	9	40.4
9	L271	T283	63.5	2	11.2
10	L75	M276	63.0	12	55.1
mean				8.0 ± 2.8	35.7 ± 13.0

TABLE 3. Pairs of amino acids i, j with the largest variation of $\Delta G_{ij}^{\alpha=1/2}$ in 6Y2G. The length of the shortest paths l_{ij} between the two nodes as well as the distance between the C_α of both amino acids, d_{ij} (Å), are also given. Amino acids in the binding site or directly bounded to a residue in it are marked in bold.

to the protease bounded to an inhibitor 25 times less potent than the one bounded to 6Y2G. The illustration of the shortest paths communicating these pairs of residues is illustrated in Fig. **4.3**.

Finally, we consider the structures of the CoV-2 M$^{\text{pro}}$ bounded to the inhibitors N3 (6LU7) and X77 (6W63). The individual transmissibility between amino acids in these two structures share some resemblances. For instance, in the top ten ranking of residue pairs based on the values of $\Delta G_{ij}^{\alpha=1/2}$ for 6LU7 appear the amino acids G183, L167, which are also ranked among the top ten for 6W63. The average length of the shortest paths between the top ten pairs of residues in 6LU7 is 7.2 ± 2.3, while that of 6W63 is 7.4 ± 2.0. The average geometric separation between the top amino acid pairs in 6LU7 is slightly smaller than that observed in 6W63 (see Tables 4 and 5).

The illustration of these paths in both structures are shown in Figs. **4.4** and **4.5**, respectively. It should be noticed that in 6LU7 these residues connect the domains II and III of the main protease or communicate residues located both in the domain III. However, in 6W63 these pairs interconnect residues in domain I with others in domain III or amino acids belonging to domains II and III.

rank	i	j	$\Delta G_{ij}^{\alpha=1/2}$	l_{ij}	d_{ij} (Å)
1	G183	N276	121.9	9	33.2
2	G183	N221	100.1	9	38.5
3	G183	L269	99.0	7	29.8
4	**L167**	M276	96.3	9	31.5
5	M276	C300	96.1	5	23.2
6	**L167**	N221	91.1	9	40.6
7	**L167**	L269	83.5	8	32.2
8	N221	C300	80.6	5	21.7
9	F3	C300	77.4	2	7.68
10	L177	N221	75.7	9	44.7
mean				7.2 ± 2.3	30.3 ± 10.1

TABLE 4. Pairs of amino acids i, j with the largest variation of $\Delta G_{ij}^{\alpha=1/2}$ in 6LU7. The length of the shortest paths l_{ij} between the two nodes as well as the distance between the C_α of both amino acids, d_{ij} (Å), are also given. Amino acids in the binding site or directly bounded to a residue in it are marked in bold.

rank	i	j	$\Delta G_{ij}^{\alpha=1/2}$	l_{ij}	d_{ij} (Å)
1	**S139**	R217	151.0	7	32.2
2	**L167**	R217	128.6	8	39.0
3	G183	R217	113.4	8	37.5
4	G71	R217	112.7	11	49.3
5	**S139**	L282	109.7	7	23.0
6	G71	**L167**	98.2	5	29.9
7	G71	M165	98.0	4	23.8
8	**L167**	L282	97.7	8	31.3
9	G71	L242	95.9	10	46.5
10	**S139**	L250	90.5	6	29.4
mean				7.4 ± 2.0	34.2 ± 8.4

TABLE 5. Pairs of amino acids i, j with the largest variation of $\Delta G_{ij}^{\alpha=1/2}$ in 6W63. The length of the shortest paths l_{ij} between the two nodes as well as the distance between the C_α of both amino acids, d_{ij} (Å), are also given. Amino acids in the binding site or directly bounded to a residue in it are marked in bold.
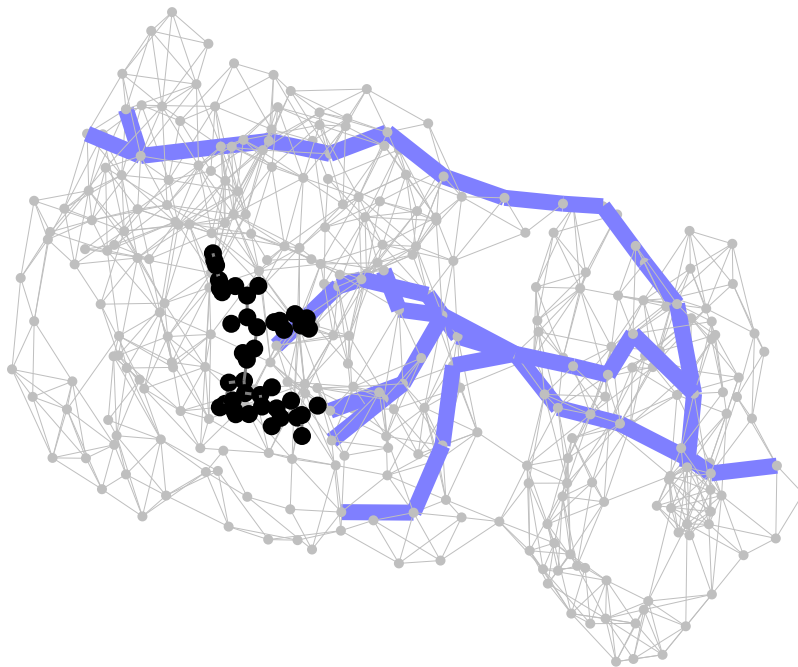
FIGURE **4.3.** Visualization of the PRN of CoV-2 main pro-
tease with inhibitor having PDB code 6Y2G. The paths
marked in blue correspond to the shortest paths between
pairs of nodes that increase their fractional communicabil-
ity respect to the free protease (see Table 3). The inhibitor
is marked in black.

5. Conclusions

There are two main conclusions in the current work. The first is that we
have proposed a generalized fractional logarithmic SI model which includes
the classical SI model as a particular case. We have found an approximate
solution to this model which represents an upper bound to its exact solution
and which under given initial conditions depends only on the Mittag-Leffler
matrix function of the adjacency matrix of the protein residue network rep-
resenting the 3-dimensional structure of the protein. The most important
characteristic of this fractional logarithmic model is that it allows to ac-
count for long-range interactions between the nodes of a network by tuning
the fractional parameter α of the model. Such long-range interactions are
of relevance in many different applications of complex systems ranging from
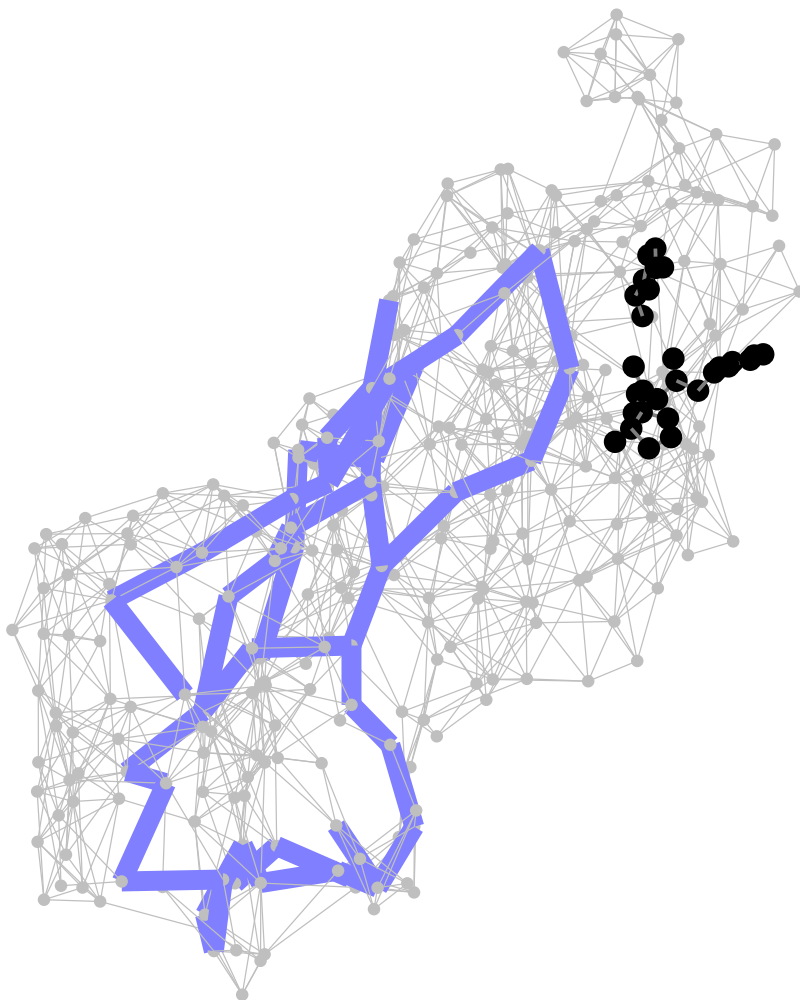biological to social systems.

FIGURE **4.4.** Visualization of the PRN of CoV-2 main protease with inhibitor having PDB code 6LU7. The paths marked in blue correspond to the shortest paths between pairs of nodes that increase their fractional communicability respect to the free protease (see Table 4). The inhibitor is marked in black.

The second main conclusion of this work is that the fractional logarithmic SI model allowed us to extract very important information about the interaction of inhibitors with the main protease of the SARS CoV-2. This structural information consists in the transmission of perturbations
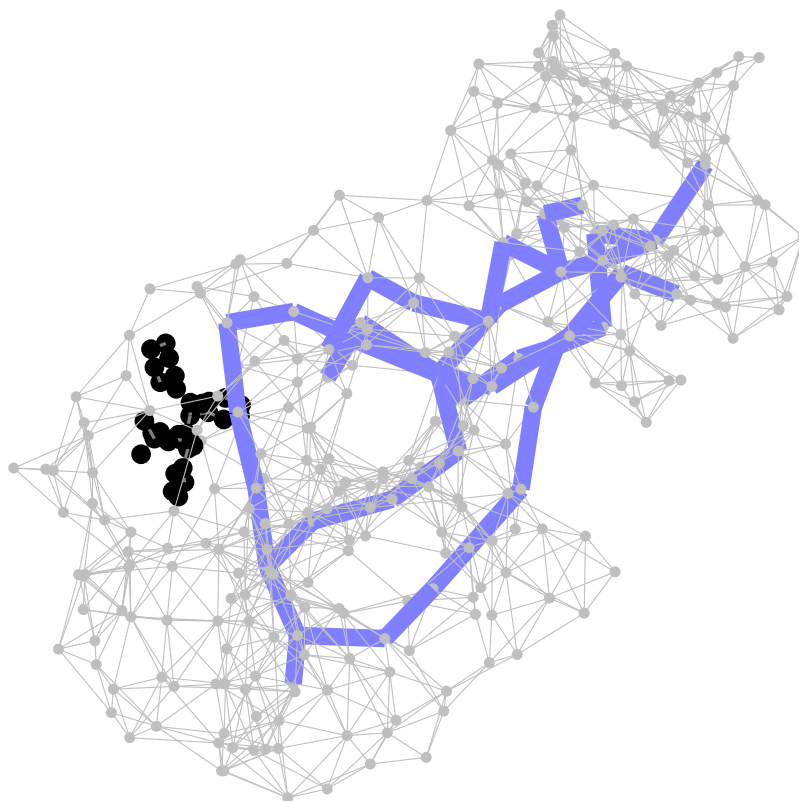
FIGURE **4.5.** Visualization of the PRN of CoV-2 main protease with inhibitor having PDB code 6W63. The paths marked in blue correspond to the shortest paths between pairs of nodes that increase their fractional communicability respect to the free protease (see Table 5). The inhibitor is marked in black.

produced by the inhibitors at the binding site of the protease to very distant amino acids in other domains of the protein. More importantly, our findings suggest that the length of this transmission seems to reflect the potency of the inhibitor. That is, the more powerful the inhibitor the longer the transmission of its effects through the protein. For instance, the very potent inhibitor O6K is able to transmit the perturbations from the binding site up to 45Å away from it as average. Other weaker inhibitors do not propagate such effect beyond 35Å from the binding site as average. Consequently, these findings are important for understanding the mechanisms of actions of such inhibitors on SARS CoV-2 M$^{\mathrm{pro}}$ and helping in the design of more potent drug candidates against this new coronavirus. Of course,

the current approach can be extended and used for the analysis of other inhibitors in other proteins not only using experimental data like in here but using computational analysis of such interactions.

Acknowledgements

References

[1] Protein data bank: the single global archive for 3D macromolecular structure data. *Nucleic acids research*, 47(D1):D520–D528, 2019.

[2] L. Abadias, E. Alvarez, et al. Uniform stability for fractional Cauchy problems and applications. *Topological Methods in Nonlinear Analysis*, 52(2):707–728, 2018.

[3] L. Abadias, C. Lizama, P. J. Miana, et al. Sharp extensions and algebraic properties for solution families of vector-valued differential equations. *Banach Journal of Mathematical Analysis*, 10(1):169–208, 2016.

[4] C. N. Angstmann, A. M. Erickson, B. I. Henry, A. V. McGann, J. M. Murray, and J. A. Nichols. Fractional order compartment models. *SIAM Journal on Applied Mathematics*, 77(2):430–446, 2017.

[5] E. Bazhlekova. The abstract Cauchy problem for the fractional evolution equation. *Fract. Calc. Appl. Anal*, 1(3):255–270, 1998.

[6] M. Benzi and P. Boito. Matrix functions in network analysis. *GAMM Mitteilungen*, 2020.

[7] H. Berry. Nonequilibrium phase transition in a self-activated biological network. *Physical review E*, 67(3):031907, 2003.

[8] A. Cooper and D. Dryden. Allostery without conformational change. *European Biophysics Journal*, 11(2):103–109, 1984.

[9] K. H. DuBay, J. P. Bothma, and P. L. Geissler. Long-range intra-protein communication can be transmitted by correlated side-chain fluctuations alone. *PLoS computational biology*, 7(9), 2011.

[10] E. Estrada. *The structure of complex networks: theory and applications*. Oxford University Press, 2012.

[11] E. Estrada. Topological analysis of SARS CoV-2 main protease. *bioRxiv*, 2020.

[12] E. Estrada and N. Hatano. Communicability in complex networks. *Physical Review E*, 77(3):036111, 2008.

[13] E. Estrada and J. A. Rodríguez-Velázquez. Subgraph centrality in complex networks. *Phys. Rev. E*, 71:056103, May 2005.

[14] E. Estrada and G. Silver. Accounting for the role of long walks on networks via a new matrix function. *Journal of Mathematical Analysis and Applications*, 449(2):1581–1600, 2017.

[15] D. Fulger, E. Scalas, and G. Germano. Monte Carlo simulation of uncoupled continuous-time random walks yielding a stochastic solution of the space-time fractional diffusion equation. *Physical Review E*, 77(2):021122, 2008.

[16] R. Garrappa and M. Popolizio. Computing the matrix Mittag-Leffler function with applications to fractional calculus. *Journal of Scientific Computing*, 77(1):129–153, 2018.

[17] G. Hu, J. Zhou, W. Yan, J. Chen, and B. Shen. The topology and dynamics of protein complexes: insights from intra–molecular network theory. *Current Protein and Peptide Science*, 14(2):121–132, 2013.

[18] Z. Jin, X. Du, Y. Xu, Y. Deng, M. Liu, Y. Zhao, B. Zhang, X. Li, L. Zhang, C. Peng, et al. Structure of Mpro from COVID-19 virus and discovery of its inhibitors. *bioRxiv*, 2020.

[19] V. Latora, V. Nicosia, and G. Russo. *Complex networks: principles, methods and applications*. Cambridge University Press, 2017.

[20] A. L. Lee et al. Frameworks for understanding long-range intra-protein communication. *Current Protein and Peptide Science*, 10(2):116–127, 2009.

[21] C.-H. Lee, S. Tenneti, and D. Y. Eun. Transient dynamics of epidemic spreading and its mitigation on large networks. In *Proceedings of the Twentieth ACM International Symposium on Mobile Ad Hoc Networking and Computing*, pages 191–200, 2019.

[22] S. Lu, M. Ji, D. Ni, and J. Zhang. Discovery of hidden allosteric sites as novel targets for allosteric drug design. *Drug discovery today*, 23(2):359–365, 2018.

[23] F. Mainardi. *Fractional calculus and waves in linear viscoelasticity: an introduction to mathematical models.* World Scientific, 2010.

[24] I. Matychyn. On computation of matrix Mittag-Leffler function. *arXiv preprint arXiv:1706.01538*, 2017.

[25] W. Mei, S. Mohagheghi, S. Zampieri, and F. Bullo. On the dynamics of deterministic epidemic propagation over networks. *Annual Reviews in Control*, 44:116–128, 2017.

[26] A. D. Mesecar. A taxonomically-driven approach to development of pot broad-spectrum inhibitors of coronavirus main proteas including SARS-Cov-2 (covid-19). *To be published*, 2020.

[27] M. Miotto, L. Di Rienzo, P. Corsi, D. Raimondo, and E. Milanetti. Simulated epidemics in 3d protein structures to detect functional properties. *arXiv preprint arXiv:1906.05390*, 2019.

[28] S. K. Mishra, M. Gupta, and D. K. Upadhyay. Fractional derivative of logarithmic function and its applications as multipurpose asp circuit. *Analog Integrated Circuits and Signal Processing*, 100(2):377–387, 2019.

[29] D. Mugnolo. Dynamical systems associated with adjacency matrices. *arXiv preprint arXiv:1702.05253*, 2017.

[30] K. M. Ottemann, W. Xiao, Y.-K. Shin, and D. E. Koshland. A piston model for transmembrane signaling of the aspartate receptor. *Science*, 285(5434):1751–1754, 1999.

[31] A. Sadeghi and J. R. Cardoso. Some notes on properties of the matrix Mittag-Leffler function. *Applied Mathematics and Computation*, 338:733–738, 2018.

[32] C. S. G. The International et al. The species severe acute respiratory syndrome-related coronavirus: classifying 2019-ncov and naming it SARS-CoV-2. *Nature Microbiology*, page 1, 2020.

[33] F. Wu, S. Zhao, B. Yu, Y.-M. Chen, et al. A new coronavirus associated with human respiratory disease in China. *Nature*, 579(7798):265–269, 2020.

[34] L. Zhang, D. Lin, X. Sun, U. Curth, C. Drosten, L. Sauerhering, S. Becker, K. Rox, and R. Hilgenfeld. Crystal structure of SARS-CoV-2 main protease provides a basis for design of improved α-ketoamide inhibitors. *Science*, 2020.

[35] P. Zhou, X.-L. Yang, X.-G. Wang, B. Hu, et al. A pneumonia outbreak associated with a new coronavirus of probable bat origin. *Nature*, 579(7798):270–273, 2020.

[1]*Departamento de Matemáticas, Facultad de Ciencias*
Universidad de Zaragoza, 50009 Zaragoza, Spain.
    e-mail: labadias@unizar.es

[2]*Instituto Universitario de Matemáticas y Aplicaciones*
Universidad de Zaragoza, 50009 Zaragoza, Spain.
    email: estrada66@unizar.es

[3]*Laboratoire Jacques-Louis Lions, Université Pierre-et-Marie-Curie (UPMC)*
4 place Jussieu, 75005, Paris, France.
    email: estradarodriguez@ljll.math.upmc.fr

[4]*ARAID Foundation, Government of Aragón*
50018 Zaragoza, Spain.
    email: estrada66@posta.unizar.es